frontiers in Materials

ORIGINAL RESEARCH
published: 15 May 2015
doi: 10.3389/fmats.2015.00040

A facile route to metal oxides/single-walled carbon nanotube macrofilm nanocomposites for energy storage

*Zeyuan Cao and Bingqing Wei**

Department of Mechanical Engineering, University of Delaware, Newark, DE, USA

Nanocomposites consisting of transition-metal oxides and carbon nanomaterials with a desired size and structure are highly demanded for high-performance energy storage devices. Here, a facile two-step and cost-efficient approach relying on directly thermal treatment of chemical vapor deposition products is developed as a general synthetic method to prepare a family of metal oxides [M_xO_y (M = Fe, Co, Ni)]/single-walled carbon nanotube (SWNT) macrofilm nanocomposites. The M_xO_y nanoparticles obtained are of 3–17 nm in diameter and homogeneously anchor on the free-standing SWNT macrofilms. NiO/SWNT also exhibits a high-specific capacitance of 400 F g^{-1} and fast charge-transfer Faradaic redox reactions to achieve asymmetric supercapacitors with a high power and energy density. All M_xO_y/SWNT nanocomposites could deliver a high capacity beyond 1000 mAh g^{-1} and show excellent cycling stability for lithium-ion batteries. The impressive results demonstrate the promise for energy storage devices and the general approach may pave the way to synthesize other functional nanocomposites.

Keywords: carbon nanotube macrofilms, metal oxides, nanocomposites, asymmetric supercapacitors, lithium-ion batteries

OPEN ACCESS

Edited by:
Mihri Ozkan, University of California Riverside, USA

Reviewed by:
Zhengjun Zhang, Tsinghua University, China
Dexian Ye, Virginia Commonwealth University, USA

***Correspondence:**
Bingqing Wei, Department of Mechanical Engineering, University of Delaware, Newark, DE 19716, USA
weib@udel.edu

Specialty section:
This article was submitted to Nanoenergy Technologies and Materials, a section of the journal Frontiers in Materials

Received: *03 March 2015*
Accepted: *29 April 2015*
Published: *15 May 2015*

Citation:
Cao Z and Wei B (2015) A facile route to metal oxides/single-walled carbon nanotube macrofilm nanocomposites for energy storage. Front. Mater. 2:40. doi: 10.3389/fmats.2015.00040

Introduction

Nanocomposites, consisting of a set of first-row transition-metal oxides such as Fe_2O_3 (Wang et al., 2012; Cao and Wei, 2013a), Fe_3O_4 (Su et al., 2011; Cao and Wei, 2013b), CoO (Guo et al., 2013), Co_3O_4 (Wu et al., 2010; Liang et al., 2012), NiO (Lee et al., 2005; Zhou et al., 2012), V_2O_5 (Cao and Wei, 2013c), and MnO_2 (Yu et al., 2011; Qin et al., 2013) in a variety of structures at nanoscale, and carbon nanomaterials such as carbon nanotubes (CNTs) and graphene, have been extensively explored and investigated for electrochemical applications, in particular, energy storage (Cao and Wei, 2013d; Xu et al., 2013). One common strategy in designing such materials is coupling size-controllable nanoparticles on the supporting carbon scaffolds to tailor surface area, conductivity, and charge-transfer interaction in order to obtain the desired characteristics such as a high energy and power density as well as a long-cycle stability (Poizot et al., 2000; Grugeon et al., 2001; Li et al., 2007). However, current synthetic methods based on such a strategy vary with specific cases and are complicated with high cost, which impedes the practical production and application. Hence, efficient, general, and robust synthesis methods are sought to address these challenges. In our previous work, we have successfully demonstrated a facile heat treatment process to convert single-walled CNT (SWNT) macrofilms, containing Fe catalysts and obtained via chemical vapor deposition (CVD), to alpha-Fe_2O_3/SWNT nanocomposites (Cao and Wei, 2013a). The resulting Fe_2O_3/SWNT nanocomposite films exhibited good electric conductivity and strain accommodation for lithium-ion batteries with a high-specific capacity (Cao and Wei, 2013a).

Herein, following the analogous formation mechanism of the Fe_2O_3/SWNT nanocomposite, we generalize this facile route to the family of M_xO_y (M = Fe, Co, Ni) with SWNT macrofilm nanocomposites for electrochemical applications. The size of M_xO_y nanoparticles is successfully controlled within 3–17 nm and the desired morphology of electrically interconnected networks that associate metal oxides with SWNT is formed. We particularly discussed an optimized asymmetric supercapacitor that consists of NiO/SWNT as the positive electrode and a pure CNT macrofilm as the negative electrode, which has shown a high specific capacitance of 130 F g^{-1} after a long-term discharge–charge duration of 5000 cycles. In addition, both of the NiO/SWNT and Co_3O_4/SWNT nanocomposites exhibit an exceptionally high capacity beyond 1000 mAh g^{-1} in Li-ion batteries.

The general approach is composed of two steps to synthesize M_xO_y/SWNT macrofilms as illustrated in **Scheme 1**. First, bis(cyclopentadienyl)metal (MCp2, M = Fe, Co, Ni) and sulfur (with an atomic ratio of M/S = 10) were mixed as precursors to produce SWNT macrofilms by CVD. Taking NiO as an example, nickelocene (NiCp2) is decomposed during the CVD reaction to Ni ions as catalyst sources and two parallel Cp rings as carbon source for SWNT formation. Sulfur is a predominant additive to control the wall number of CNTs so that to promote SWNT growth as well as to enhance the growth rate. The deposition lasted for half an hour at 1100°C and the as-prepared SWNT macrofilms were not achieved until cooled down to room temperature followed by the second step, calcination in air. The heat treatment resulted in the oxidation of the metal catalysts to metal oxides and also the growth of the oxides. The detailed synthetic procedures are described in the following section.

Materials and Methods

Synthesis of M_xO_y (M = Fe, Co, Ni)/SWNT Macrofilm Nanocomposites

Single-walled carbon nanotube (SWNT) macrofilms were synthesized by the modified floating CVD method reported in the previously published work (Zhu and Wei, 2007). In brief, a mixture of bis(cyclopentadienyl)metal (MCp2, M = Fe, Co, Ni) and sulfur (atomic ratio M:S = 1:10, both from Sigma Aldrich) as precursors in a crucible boat was placed at the inlet of a ceramic tube of an electric furnace. The furnace was pre-heated to 1100–1150°C with an argon gas flow of 500 mL min^{-1}. Meanwhile, the MCp2 with a relatively low sublimation point (~100°C) was introduced by the Ar carrier gas flow into the central reaction zone of the furnace. During the deposition, a mixed gas flow of Ar (1500 mL min^{-1}) and H_2 (150 mL min^{-1}) was delivered and the MCp2 then started pyrolysis at such a high temperature to generate carbon source and metal catalysts for CNT growth. It was widely recognized that sulfur is indispensable in controlling the wall number of CNTs. Sulfur acts as an additive to promote SWNT growth as well as to enhance the growth rate of SWNTs. After a 30 min reaction, large-area SWNT macrofilms [M-CNT (M = Fe, Co, Ni)] containing metal catalysts with uniformity (randomly homogeneous entanglement of SWNT bundles) and conformability (distribution of the nanotube diameter ranges from 0.8 to 1.3 nm) could be collected from the entire furnace tube. It is the result of a reverse gas flow generated from the central hot zone to the cold ends caused by the pressure difference (Cao and Wei, 2013d). The thickness of the films can be controlled by mainly adjusting the amount of the precursor mixtures and reaction time. The M-CNT macrofilms were peeled off from the tube walls when the furnace was cooled down. Subsequently, the direct thermal treatment was performed to the M-CNT by calcination in air for 30 min below the critical temperature that CNT began to burn out (about 450°C). During the heat treatment, metal catalysts were oxidized to metal oxide nanoparticles with fine sizes. Three samples of Co_3O_4/SWNT were prepared at different annealing temperatures: Co-CNT (100°C), Co_3O_4/SWNT (200°C), and Co_3O_4/SWNT (400°C) because of the more complicated phases than NiO/SWNT, which was obtained by annealing only at 400°C.

Structural Characterization

Morphological and structural characterizations were performed using transmission electron microscope (TEM) and high-resolution TEM (HRTEM) on JEOL JEM-2010F field emission TEM operating at 200 kV. The crystalline phase of the samples was determined using X-ray diffraction (XRD) collected on a Philips X'Pert powder diffractometer with Cu

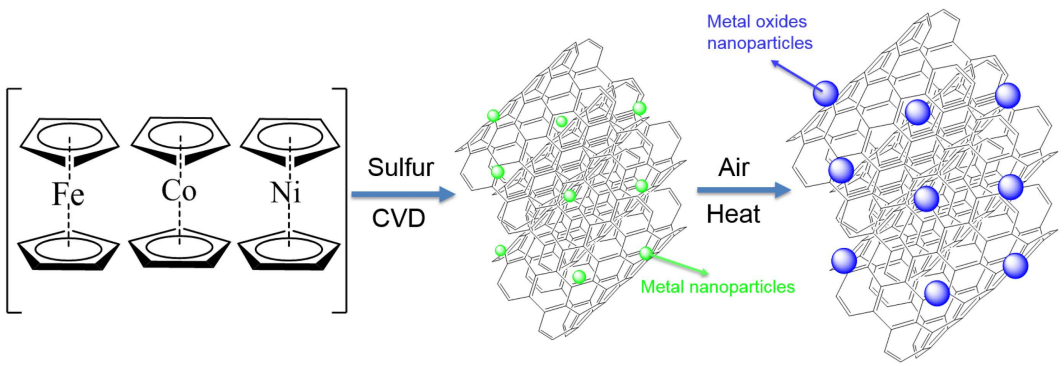

SCHEME 1 | Two-step synthetic route to M_xO_y (M = Fe, Co, Ni)/SWNT macrofilm nanocomposites.

Kα radiation (λ = 0.15418 nm) operating at 45 kV and 40 mA. Raman spectroscopy (Bruker SENTERRA with 532 nm laser excitation) was employed to verify the transformation of metal catalysts to metal oxides. The thermogravimetric analysis (TGA) was carried out on a Mettler Toledo TGA/DSA 1 STARe System under air flow (20 mL min^{-1}) with a heating rate of 5°C min^{-1}.

Lithium-Ion Battery Electrochemical Measurements

The total mass of free-standing M_xO_y/SWNT films as working electrodes were weighed by a micro/ultramicro balance (Mettler Toledo XP6) with 0.001 mg accuracy. CR2032 coin cells were assembled under a half-cell system with lithium ribbons (0.38 mm thick, 99.9%, Sigma Aldrich) as both counter and reference electrodes in an argon-filled glovebox (MBRAUN UNIlab). Celgard 2500 were used as separators. Electrolyte is 1 M $LiPF_6$ dissolved in 1:1 (v/v) ethylene carbonate (EC): diethyl carbonate (DEC) (Ferro Co.). The CV curves were collected by PARSTAT 2273 (Princeton Applied Research) potentiostat/galvanostat. The galvanostatic discharge–charge tests were carried out using BT-4 four-channel battery test equipment (Arbin Instrument, Ltd.).

Asymmetric Supercapacitor Electrochemical Measurements

Similarly, the free-standing NiO/SWNT macrofilms were employed as working electrodes. The CV tests of the NiO/SWNT electrodes were performed on the potentiostat PARSTAT 2273 (Princeton Applied Research) in a three-electrode cell. Pt wire was used as the counter electrode and Ag/AgCl electrode as reference electrode. The specific capacitance of the electrode can be calculated from the CV curves according to the following equation:

$$C = \frac{\int i\mathrm{d}V}{\nu \Delta V} \tag{1}$$

where C is the specific capacitance (faraday per gram) based on the mass of the active materials, i is the current density response (with the unit of ampere per gram. $i = I/m$, I is the current response in ampere), ΔV is the voltage window of CV, ν is the scan rate. To assemble an asymmetric supercapacitor, the loading mass ratio between NiO/SWNT (+) as positive electrode and purified SWNT (−) as negative electrode was estimated to be 0.25 from the equation:

$$\frac{m_+}{m_-} = \frac{C_- \Delta E_-}{C_+ \Delta E_+} \tag{2}$$

where m is the mass, C is the specific capacitance and ΔE is the potential window for electrodes on each side. The subscripts of + and − represent the positive and negative electrodes, respectively. The electrochemical measurements of the asymmetric supercapacitor were carried out at room temperature under a two-electrode configuration in a CR2032 coin cell with Whatman® glass microfiber filter as separator in 1 M KOH aqueous electrolyte. The cycling performance was measured by galvanostatic discharge–charge tests on BT-4 four-channel battery test equipment (Arbin Instrument, Ltd.). The specific capacitance could be also calculated by:

$$C = \frac{i\Delta t}{\Delta V} \tag{3}$$

where i is the galvanostatic charge/discharge current density (ampere per gram), Δt is the time for a full discharge in one cycle, ΔV is the voltage window delimited for charge/discharge cycling.

Results and Discussion

The size, morphology, and structure of the resulting materials were characterized using TEM. TEM images show size distribution of the Co_3O_4 nanoparticles in the range of 5–17 nm (**Figure 1A**) and the NiO nanoparticles with a diameter of 3–10 nm (**Figure 1D**). It is noted that the isolated-dispersed tiny particles in **Figure 1A** are Co catalysts, implying an incomplete oxidization at the low temperature of 200°C. In contrast, NiO has a better uniformity with a narrow size distribution due to complete transformation to NiO nanoparticles at a higher temperature of 400°C. It was confirmed that the Co residues in the Co_3O_4/SWNT sample (200°C) could be further oxidized when they were heated at 400°C in air. **Figures 1B,E** show similar morphologies of the M_xO_y/SWNT macrofilm nanocomposites. Metal oxide nanoparticles are coupled with the entangled serpentine CNT bundles. HRTEM images (**Figures 1C,F**) reveal the well-defined lattice fringes corresponding to face-centered cubic Co_3O_4 and NiO, respectively. TGA (shown in **Figure 2A**) demonstrates 23 wt. % CNT in the Co_3O_4/SWNT nanocomposite (200°C) while the NiO/SWNT nanocomposite contains only 12 wt. % carbon scaffold.

X-ray diffraction and Raman spectroscopy further confirm the transformation from metal catalysts to metal oxides during calcination. The XRD patterns before and after heat treatments are shown in **Figures 2B,C**. The results indicate that the crystal structure of Co_3O_4 is cubic phase with *Fd-3m* space group according to JCPDS No. 42-1467 and NiO is of the natural Brunsenite phase with *Fm-3m* space group (JCPDS No. 47-1049). This is in a good agreement with the HRTEM observations. Consistently, two distinct phases, Co_3O_4 (marked by asteroid) and pure Co (marked by spade) are present in the XRD pattern of the Co_3O_4/SWNT sample (200°C). The absence of Co diffraction peaks in the Co_3O_4/SWNT sample annealed at 400°C confirms the complete oxidation of the Co catalysts. Raman spectra (**Figure 2D**) show the RBM features of SWNT for all the samples at the wavenumber of ~100 cm^{-1} as well as the typical D and G modes at 1350 and 1587 cm^{-1}, consistent with the TEM results (Jorio et al., 2003). The presence of two small peaks, E_g (488 cm^{-1}) and F_{2g} (522 cm^{-1}) separate at each side of 500 cm^{-1} with F_{2g} (618 cm^{-1}) and the strongest peak A_{1g} (691 cm^{-1}) are typically indicative of the Co_3O_4 formation after the heat treatment (Hadjiev et al., 1988). Likewise, the first-order transverse optical (TO, 404 cm^{-1}), longitudinal optical (LO, 564 cm^{-1}), and two two-photon (2TO at 705 cm^{-1}, 2LO at 1080 cm^{-1}) peaks belong to NiO nanoparticles (Wang et al., 2002; Zhou et al., 2012).

The electrochemical performance was studied in a half cell that consists of the free-standing M_xO_y/SWNT macrofilms as working

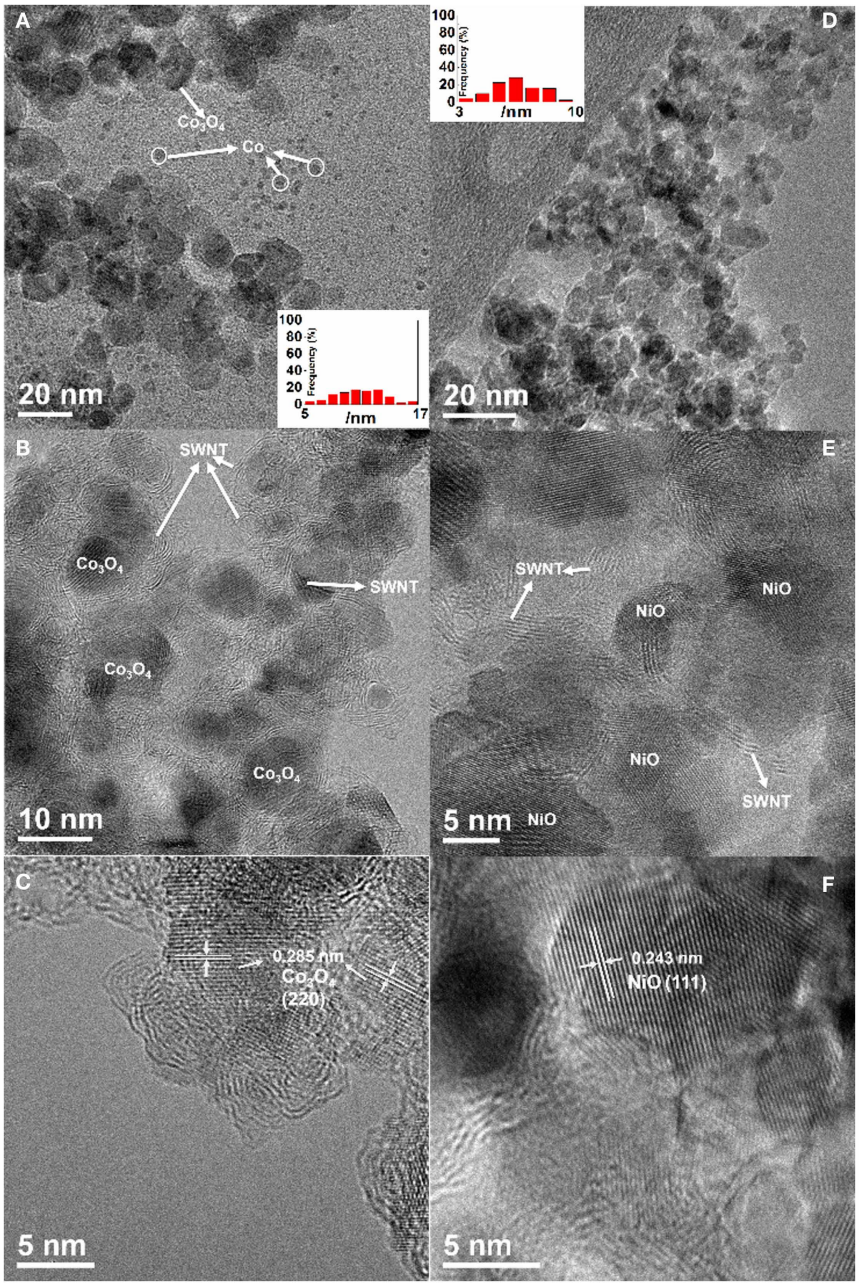

FIGURE 1 | **(A,B,D,E)** TEM and **(C,F)** HRTEM images of **(A–C)** Co_3O_4/SWNT (200°C) and **(D–F)** NiO/SWNT. Insets: histograms of the nanoparticle size distribution.

electrodes and lithium metal as both counter and reference electrode under a two-electrode configuration. Cyclic voltammetry (CV) was performed at an extremely slow scan rate of 0.1 mV s^{-1} to adapt to the sluggish kinetics of lithiation/delithiation. The CV plot (**Figure 3A**) exhibits the first two cycles for M_xO_y/SWNT in fresh cells. The cathodic peaks at the potential higher than 1 V vs. Li^+/Li on the first-cycle curves for both samples are ascribed to the formation of a solid electrolyte interface (SEI) film (Varghese et al., 2008; Zhou et al., 2012). The disappearance of them in the second cycle indicates the irreversible processes of SEI (Guo et al., 2013). The peaks with a maximum current at 0.45 and 0.87 V for NiO/SWNT and Co_3O_4/SWNT, respectively, are assigned to the reduction of M ions to M^0 according to conversion reactions ($2y\text{Li} + M_xO_y \leftrightarrow x\text{M} + y\text{Li}_2\text{O}$) (Taberna et al., 2006). Both the reactions shift to a more positive potential on the CV curves in the following cycles. The difference in the number of the cathodic peaks (one at 1 V for NiO/SWNT, two at 0.9 and 1.36 V for Co_3O_4/SWNT) suggests the different reduction steps from the single oxidized state of Ni (II) in NiO and the multi-oxidized states of Co (II or III) in Co_3O_4, which agrees with the previously reported

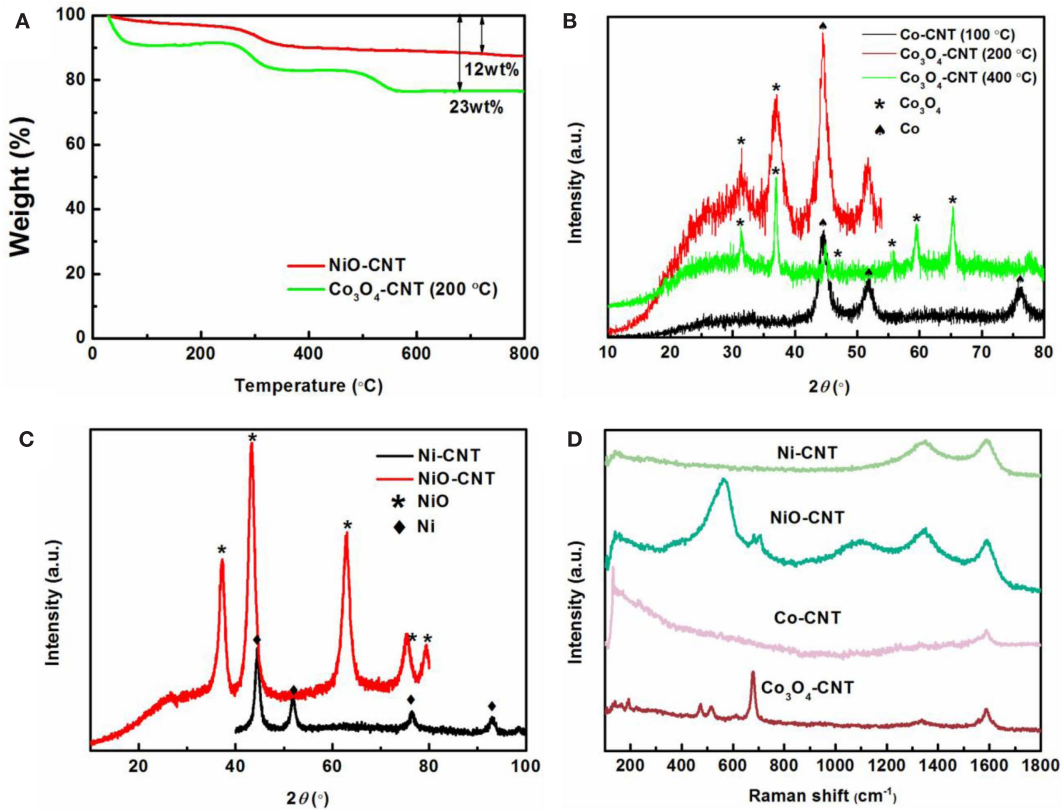

FIGURE 2 | **(A)** TGA curves of NiO/SWNT and Co_3O_4/SWNT (200°C). **(B)** XRD patterns of Co-CNT (100°C), Co_3O_4/SWNT (200, 400°C). **(C)** XRD patterns of Ni-CNT and NiO/SWNT. **(D)** Raman spectra of Co-CNT (100°C), Co_3O_4/SWNT (200, 400°C), Ni-CNT, and NiO/SWNT.

results of Fe_2O_3 (Cao and Wei, 2013a). Afterwards, the subsequent galvanostatic discharge/charge cycling measurements were carried out between 0.001 and 3 V at a constant current density of 50 mA g^{-1} with the same samples. **Figure 3B** shows their discharge/charge voltage profiles. Consistent with CV analysis, two plateaus at ~1.5 and ~1 V on the discharge curve of Co_3O_4/SWNT were observed corresponding to the two cathodic peaks, while NiO/SWNT has one plateau at ~1 V during discharge. A common discharge tail in the low voltage region between 0.8 and 0.001 V with more inclined slope is present for M_xO_y/SWNT, which is attributed to the partial capacity contribution from the SWNT macrofilms. Upon charging, there are two plateaus for both samples, which originate from the reverse processes of the conversion reactions from M^0 to M_xO_y (Varghese et al., 2008). For Co_3O_4/SWNT, they (1.26 and 2 V) correspond to the two anodic peaks at 1.28 and 2 V on the CV curve. By contrast, NiO/SWNT has the higher ones at 1.32 and 2.2 V corresponding to peaks (1.39 and 2.22 V) in the CV plot. The continuous cycling results of NiO/SWNT over 80 cycles are selectively recorded in every 10 cycles as shown in **Figures 3C,D**. Basically, the discharge/charge curves are almost overlapped (**Figure 3C**), indicating a good cyclic stability. The discharge capacity maintains at 894 mAh g^{-1} after 80 cycles with a retention as high as 88%. Compared with non-free-standing NiO/graphene (883 mAh g^{-1} after 50 cycles) (Zhou et al., 2012) and Co_3O_4/graphene (~935 mAh g^{-1} after 30 cycles) (Wu et al., 2010) nanocomposites prepared by the cumbersome synthesis, to the best of our knowledge, the M_xO_y/SWNT nanocomposites (over 1000 mAh g^{-1}) demonstrate one of the best electrochemical performance with an additional binder-free benefit among the reported hybrid anode materials.

In spite of the higher energy density, lithium-ion batteries usually suffer from a lower power density than supercapacitors. Taking advantage of both virtues of these two energy storage devices, we turn to an alternative approach to compose the asymmetric supercapacitors with a battery-type Faradaic electrode (as the energy source) and a capacitor-type electrode (as the power source) (Yan et al., 2012). They can extend operation voltage in the cell system with aqueous electrolyte beyond the water splitting limit (~1.23 V) by making full use of the two electrodes at different potential windows, consequently resulting in an enhanced specific capacitance and significantly improved energy density (Yan et al., 2012). **Figure 4A** shows the typical CV curves of the NiO/SWNT nanocomposite at different scan rates in 1 M KOH aqueous solution. All the CV curves have a pair of strong redox peaks, which are representative of the pseudo-capacitive behavior due to Faradaic redox reactions. This is distinct from an approximately ideal rectangular shape of CV curves for electric double layer capacitors. The redox couple, for example, located at around 0.27 V (cathodic)/0.35 V (anodic) vs.

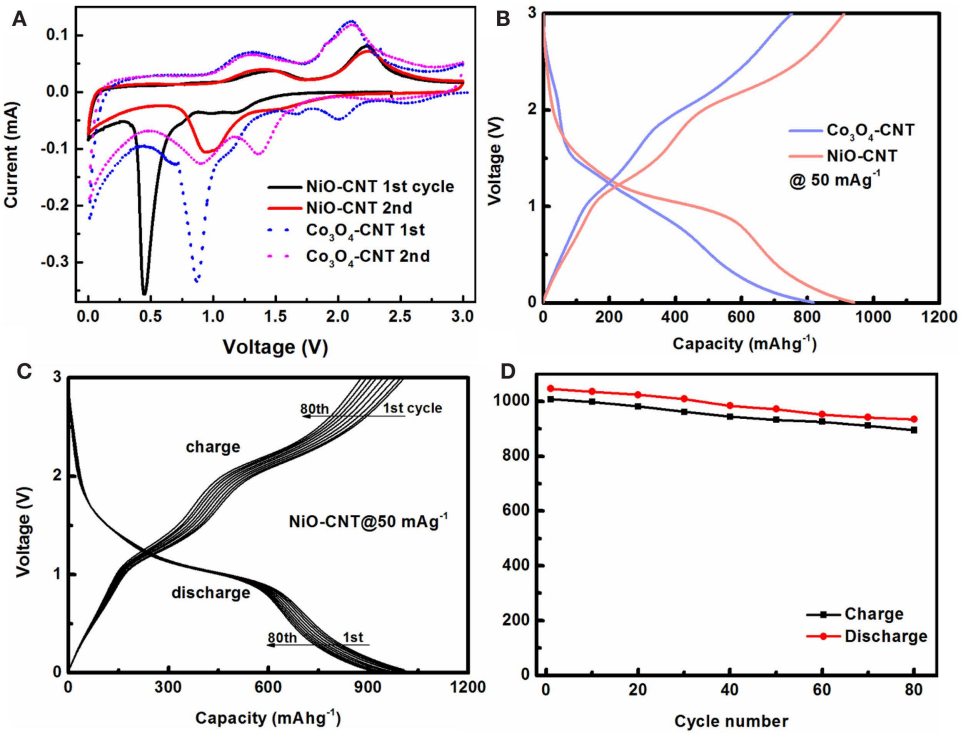

FIGURE 3 | **Lithium-ion battery performance of MxOy/SWNT in half cells**. **(A)** CV curves at a slow scan rate of 0.1 mV s^{-1}, and **(B)** galvanostatic discharge/charge voltage profiles at a constant current density of 50 mA g^{-1} after CV tests of Co_3O_4/SWNT and NiO/SWNT. **(C)** Discharge/charge curves at the selected cycles, **(D)** cycling performance of NiO/SWNT electrodes.

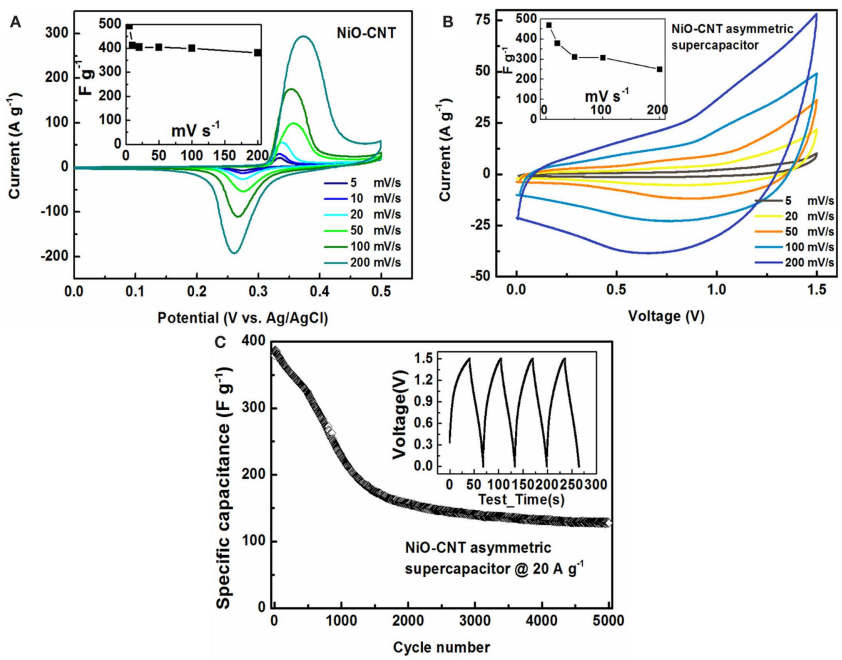

FIGURE 4 | **(A)** CV curves of NiO/SWNT at various scan rates. Inset: specific capacitance as a function of the scan rates calculated from CV. **(B)** CV curves of an asymmetric supercapacitor composed of (+) NiO/SWNT-SWNT (–) at different scan rates between 5 and 200 mV s^{-1}. Inset: specific capacitance vs. scan rates. **(C)** Galvanostatic charge/discharge cyclic performance of the asymmetric supercapacitor within a voltage window of 1.5 V at a current density of 20 A g^{-1}. Inset: charge/discharge curves.

Ag/AgCl at the scan rate of 50 mV s^{-1}, is attributed to the reversible Faradaic redox reactions between NiO and NiOOH according to the equation: $NiO + OH^- - e^- \leftrightarrow NiOOH$ (Lu et al., 2011). The specific capacitance of the NiO/SWNT electrodes as a function of scan rates calculated from the CV curves (inset of **Figure 4A**) is stable at ~400 F g^{-1}, suggesting the fast charge transfer in the Faradaic processes (Yan et al., 2012). Purified SWNT macrofilms without metal oxide nanoparticles, which deliver a specific capacitance of ~40 F g^{-1} as described in previous work (Yu et al., 2009), are employed as negative electrodes to assemble the asymmetric supercapacitors in 1 M KOH aqueous electrolyte with the NiO/SWNT positive electrodes by carefully matching their mass ratio (see Section "Materials and Methods" for details). **Figure 4B** exhibits the CV curves of the asymmetric supercapacitor at various scan rates from 5 to 200 mV s^{-1} within an operation voltage window of 1.5 V. The specific capacitance of the asymmetric cell (based on the total mass of the two electrodes) maintains as high as 249 F g^{-1} at 200 mV s^{-1} from 468 F g^{-1} at 5 mV s^{-1} as the scan rate increases. The galvanostatic charge/discharge curves at a current density of 20 A g^{-1} (inset of **Figure 4C**) show a good linear correlation of voltage with time, confirming a rapid *I–V* response of NiO/SWNT (Fan et al., 2011). The nearly equilateral triangular shapes demonstrate the excellent electrochemical reversibility. It is worth noting that at such a high-current density, the specific capacitance approaches a steady state during long-life cycling up to 5000 cycles. The performance above 130 F g^{-1} is sufficiently high to enable the asymmetric supercapacitor with qualified high energy and power density for durable and practical applications.

Conclusion

In summary, we have developed a general and facile strategy for synthesizing M_xO_y (M = Fe, Co, Ni)/SWNT macrofilm nanocomposites via CVD growth followed by a thermal treatment. We have successfully demonstrated their promise in energy storage. NiO/SWNT exhibits an excellent electrochemical performance in asymmetric supercapacitors with a high power and energy density. All M_xO_y/SWNT have shown a high-specific capacity and cycling stability for lithium-ion batteries. This work proposed an important family of material candidates to serve lithium-ion battery industry. It may also stimulate the evolution of new technique involving production of many advanced, low-cost transitional metal oxide nanocomposites for electrochemical applications.

Acknowledgments

The authors gratefully acknowledge the financial supports from the US National Science Foundation (NSF) under the contract of 1067947 and AFOSR MURI-FA9550-12-1-0035.

References

Cao, Z., and Wei, B. Q. (2013a). α-Fe_2O_3/single-walled carbon nanotube hybrid films as high-performance anodes for rechargeable lithium-ion batteries. *J. Power Sources* **241**, 330. doi:10.1016/j.jpowsour.2013.04.101

Cao, Z., and Wei, B. Q. (2013b). High rate capability of hydrogen annealed iron oxide-single walled carbon nanotube hybrid films for lithium-ion batteries. *ACS Appl. Mater. Interfaces* **5**, 10246. doi:10.1021/am403028z

Cao, Z., and Wei, B. Q. (2013c). V_2O_5/single-walled carbon nanotube hybrid mesoporous films as cathodes with high-rate capacities for rechargeable lithium ion batteries. *Nano Energy* **2**, 481. doi:10.1016/j.nanoen.2012.11.013

Cao, Z., and Wei, B. Q. (2013d). A perspective: carbon nanotube macro-films for energy storage. *Energy Environ. Sci.* **6**, 3183. doi:10.1039/C3EE42261E

Fan, Z., Yan, J., Wei, T., Zhi, L., Ning, G., Li, T., et al. (2011). Asymmetric supercapacitors based on graphene/MnO_2 and activated carbon nanofiber electrodes with high power and energy density. *Adv. Funct. Mater.* **21**, 2366. doi:10.1002/adfm.201100058

Grugeon, S., Laruelle, S., Herrera-Urbina, R., Dupont, L., Poizot, P., and Tarascon, J.-M. (2001). Particle size effects on the electrochemical performance of copper oxides toward lithium. *J. Electrochem. Soc.* **148**, A285. doi:10.1149/1.1353566

Guo, S., Zhang, S., Wu, L., and Sun, S. (2013). Co/CoO nanoparticles assembled on graphene for electrochemical reduction of oxygen. *Angew. Chem. Int. Ed. Engl.* **124**, 11940. doi:10.1002/ange.201206152

Hadjiev, V., Iliev, M., and Vergilov, I. (1988). The Raman spectra of Co_3O_4. *J. Phys. C Solid State Phys.* **21**, L199. doi:10.1088/0022-3719/21/7/007

Jorio, A., Pimenta, M., Souza Filho, A., Saito, R., Dresselhaus, G., and Dresselhaus, M. (2003). Characterizing carbon nanotube samples with resonance Raman scattering. *New J. Phys.* **5**, 139. doi:10.1088/1367-2630/5/1/139

Lee, J. Y., Liang, K., An, K. H., and Lee, Y. H. (2005). Nickel oxide/carbon nanotubes nanocomposite for electrochemical capacitance. *Synth. Met.* **150**, 153. doi:10.1016/j.synthmet.2005.01.016

Li, J., Tang, S., Lu, L., and Zeng, H. C. (2007). Preparation of nanocomposites of metals, metal oxides, and carbon nanotubes via self-assembly. *J. Am. Chem. Soc.* **129**, 9401. doi:10.1021/ja071122v

Liang, Y., Wang, H., Diao, P., Chang, W., Hong, G., Li, Y., et al. (2012). Oxygen reduction electrocatalyst based on strongly coupled cobalt oxide nanocrystals and carbon nanotubes. *J. Am. Chem. Soc.* **134**, 15849. doi:10.1021/ja305623m

Lu, Q., Lattanzi, M. W., Chen, Y., Kou, X., Li, W., Fan, X., et al. (2011). Supercapacitor electrodes with high-energy and power densities prepared from monolithic NiO/Ni nanocomposites. *Angew. Chem. Int. Ed. Engl.* **123**, 6979. doi:10.1002/ange.201103449

Poizot, P., Laruelle, S., Grugeon, S., Dupont, L., and Tarascon, J. M. (2000). Nano-sized transition-metal oxides as negative-electrode materials for lithium-ion batteries. *Nature* **407**, 496. doi:10.1038/35035045

Qin, J., Zhang, Q., Cao, Z., Li, X., Hu, C., and Wei, B. Q. (2013). MnO_2/SWCNT macro-films as flexible binder-free anodes for high-performance Li-ion batteries. *Nano Energy* **2**, 733. doi:10.1016/j.nanoen.2012.12.009

Su, J., Cao, M., Ren, L., and Hu, C. (2011). Fe_3O_4–graphene nanocomposites with improved lithium storage and magnetism properties. *J. Phys. Chem. C* **115**, 14469. doi:10.1021/jp201666s

Taberna, P. L., Mitra, S., Poizot, P., Simon, P., and Tarascon, J. M. (2006). High rate capabilities Fe_3O_4-based Cu nano-architectured electrodes for lithium-ion battery applications. *Nat. Mater.* **5**, 567. doi:10.1038/nmat1672

Varghese, B., Reddy, M., Yanwu, Z., Lit, C. S., Hoong, T. C., Subba Rao, G., et al. (2008). Fabrication of NiO nanowall electrodes for high performance lithium ion battery. *Chem. Mater.* **20**, 3360. doi:10.1021/am100791z

Wang, W., Liu, Y., Xu, C., Zheng, C., and Wang, G. (2002). Synthesis of NiO nanorods by a novel simple precursor thermal decomposition approach. *Chem. Phys. Lett.* **362**, 119. doi:10.1016/S0009-2614(02)00996-X

Wang, Z., Luan, D., Madhavi, S., Hu, Y., and Lou, X. W. (2012). Assembling carbon-coated α-Fe_2O_3 hollow nanohorns on the CNT backbone for superior lithium storage capability. *Energy Environ. Sci.* **5**, 5252. doi:10.1039/C1EE02831F

Wu, Z.-S., Ren, W., Wen, L., Gao, L., Zhao, J., Chen, Z., et al. (2010). Graphene anchored with Co_3O_4 nanoparticles as anode of lithium ion batteries with enhanced reversible capacity and cyclic performance. *ACS Nano* **4**, 3187. doi:10.1021/nn100740x

Xu, C., Xu, B., Gu, Y., Xiong, Z., Sun, J., and Zhao, X. (2013). Graphene-based electrodes for electrochemical energy storage. *Energy Environ. Sci.* **6**, 1388. doi:10.1039/c3ee23870a

Yan, J., Fan, Z., Sun, W., Ning, G., Wei, T., Zhang, Q., et al. (2012). Advanced asymmetric supercapacitors based on $Ni(OH)_2$/graphene and porous graphene electrodes with high energy density. *Adv. Funct. Mater.* **22**, 2632. doi:10.1002/adfm.201102839

Yu, C., Masarapu, C., Rong, J., Wei, B., and Jiang, H. (2009). Stretchable supercapacitors based on buckled single-walled carbon nanotube macrofilms. *Adv. Mater.* **21**, 4793–4797. doi:10.1002/adma.200901775

Yu, G., Hu, L., Liu, N., Wang, H., Vosgueritchian, M., Yang, Y., et al. (2011). Enhancing the supercapacitor performance of graphene/MnO_2 nanostructured electrodes by conductive wrapping. *Nano Lett.* **11**, 4438. doi:10.1021/nl2026635

Zhou, G., Wang, D.-W., Yin, L.-C., Li, N., Li, F., and Cheng, H.-M. (2012). Oxygen bridges between NiO nanosheets and graphene for improvement of lithium storage. *ACS Nano* **6**, 3214. doi:10.1021/nn300098m

Zhu, H., and Wei, B. (2007). Direct fabrication of single-walled carbon nanotube macro-films on flexible substrates. *Chem. Commun. (Camb.)* **29**, 3042–3044. doi:10.1039/b702523h

Conflict of Interest Statement: The authors declare that the research was conducted in the absence of any commercial or financial relationships that could be construed as a potential conflict of interest.